Anisotropically Stiff 3D Micropillar Niche Induces Extraordinary Cell Alignment and Elongation

Yunus Alapan, Mousa Younesi, Ozan Akkus, and Umut A. Gurkan**

Cells sense their physical environment and convert biophysical cues into intracellular signals, which results in regulation of adhesion, morphology, and differentiation characteristics.[1,2] It has been shown that substrate properties, such as stiffness, control cell morphology, elongation, alignment (spatial orientation), and anisotropy of cell, and nucleus shape, which partially direct the cell fate.[3–9] Thus, it is of utmost importance to achieve elongated and aligned cellular organization in vitro for functional and hierarchical study of cell behavior. Previously, methods exploiting substrate topography were utilized to achieve cellular alignment, using techniques, such as electrospinning,[10–12] electrochemical compaction,[13,14] and microfabricated grooves and pillars.[15–19] Even though these approaches have advanced our understanding of cell–substrate interactions, they are limited to 2D planar substrates.[10–18]

In native tissues, cells are confined by extracellular matrix (ECM) and other neighboring cells from all sides and they present different morphology, adhesion, migration, and cytoskeletal arrangement in comparison to cells cultured on 2D surfaces.[20–26] The effects of substrate topography and directional stiffness properties on cell morphology, adhesion, and elongation have not been studied comprehensively in 3D environment. In the literature, Legant et al.[21] studied traction forces of different cell types in synthetic 3D hydrogels. Other studies utilized microtubes formed by rolled-up nanomembranes for 3D confinement of single cells.[20,27,28] Xi et al. studied cell mitosis in microtubes and found a correlation between chromosome segregation errors and confinement degree.[28] Koch et al. utilized glass microtubes to investigate neural stem cell migration and reported lack of lamellipodia protrusions in microtubes, in contradiction to traditional 2D planar cell culture substrates.[27] Intricate and coupled mechanical and biochemical structure of the in vivo 3D microenvironment of cells in tissues is too complicated for controlled analysis of these effects. Thus, there is still a need for engineered platforms which provide a 3D microenvironment, with precise control over topography and stiffness.

Microengineered substrates allow simplification and decoupling of the complex in vivo 3D environment by mimicking key physical characteristics, such as stiffness and directionality.[23,24] Micropillar arrays have been utilized as 2D semicontinuous substrates for studying the relationship between focal adhesion size and traction forces,[29] cell differentiation in response to substrate rigidity,[7] and induced shear forces at cell–cell junctions during neutrophil transmigration across endothelium.[30] Pillar arrays with directional stiffness have been employed as a 2D substrate to study cell adhesion, traction forces, and migration.[6,31] Microfabricated pillar substrates can be engineered to provide 3D microenvironments with controlled substrate topography, and mechanical, chemical, and biological features.

Here, we have designed and fabricated, anisotropically stiff micropillar array substrates to confine, align, and elongate single human mesenchymal stem cells (hMSCs) and cardiomyocytes in a 3D microenvironment. We present for the first time, to the best of our knowledge, control of cell elongation and alignment in a 3D microenvironment by systematically modulating the stiffness anisotropy (SA) of the microfabricated substrate. We discovered that anisotropically stiff micropillar substrates provide cellular confinement in 3D, aligning cells in the stiffer direction with extraordinary elongation of both hMSCs (≈600 µm) and cardiomyocytes (≈500 µm).

The microengineered pillar platform was composed of microscale square-shaped poststructures with 15 µm height, and varying dimension resulting in different directional stiffness levels. A uniqueness of the approach presented here is rendering the top surfaces of micropillars nonadhesive via contact printing with a surfactant, unlike earlier reports that employed micropillar structures with functionalization of the top surfaces.[29,32,33] In this study, sidewalls of the micropillars were uniquely functionalized to allow adhesion of cells in the interpillar space only (**Figure 1** and Figure S1, Supporting Information). The square geometry of the isotropically stiff pillars provided identical bending stiffness about the two orthogonal axes. We observed that micropillar substrate with isotropic stiffness induced cells to align and elongate randomly in horizontal or vertical directions (Figure 1a and Figure S2, Supporting Information). Stiffness anisotropy was introduced by varying the square pillar geometry to rectangular form, creating a stiff and a compliant pillar bending axes. Stiffness anisotropy of the substrate transformed the random alignment (either in horizontal or vertical) of cells in square micropillar array substrate (Figure 1a) to

Y. Alapan, M. Younesi, Prof. O. Akkus, Prof. U. A. Gurkan
Mechanical and Aerospace Engineering Department
Case Western Reserve University
Cleveland, OH 44106, USA
E-mail: ozan.akkus@case.edu; umut@case.edu
Prof. O. Akkus, Prof. U. A. Gurkan
Biomedical Engineering Department
Case Western Reserve University
Cleveland, OH 44106, USA
Prof. O. Akkus, Prof. U. A. Gurkan
Department of Orthopedics
Case Western Reserve University
Cleveland, OH 44106, USA
Prof. U. A. Gurkan
Advanced Platform Technology Center
Louis Stokes Cleveland Veterans Affairs Medical Center
Cleveland, OH 44106, USA

DOI: 10.1002/adhm.201600096

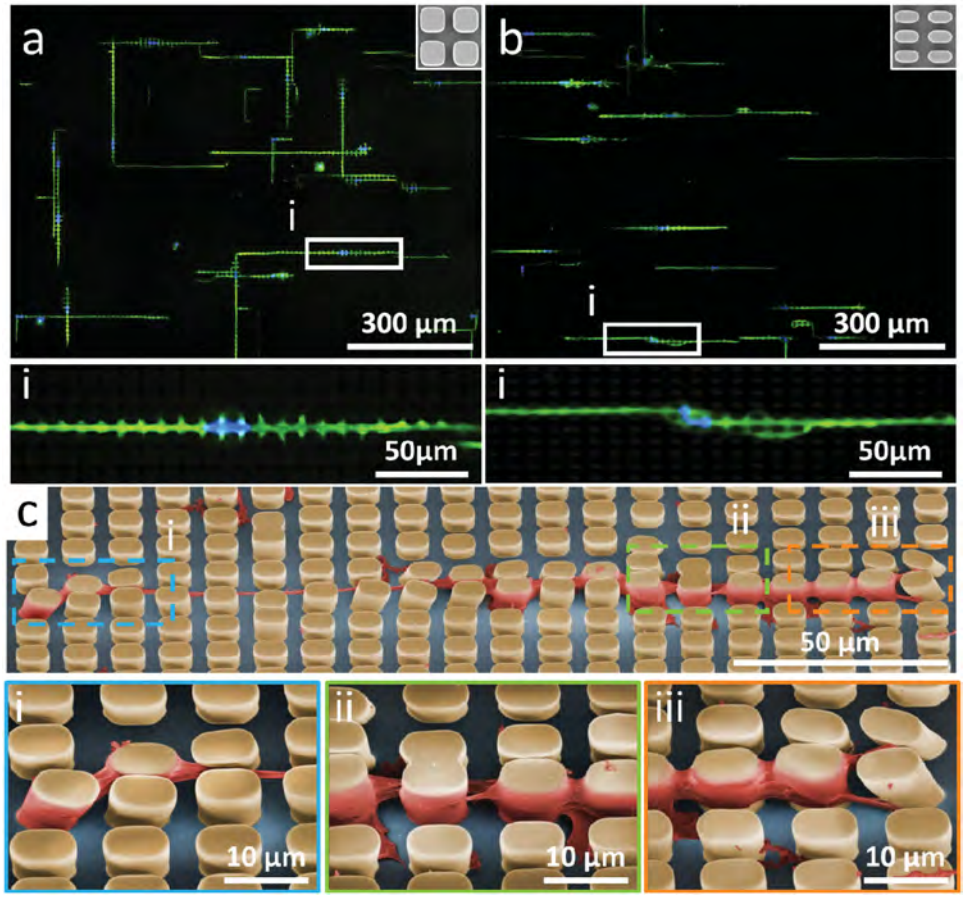

Figure 1. Unidirectional cell elongation and anisotropy using anisotropically stiff micropillar arrays. a,b) Cells (F-actin, green) and their nuclei (4′,6-diamidinp-2-phenylindole (DAPI), blue) display elongation in both a) isotropic and b) anisotropic 3D micropillar environment. Top surfaces of micropillars are rendered nonadhesive via surface chemistry. Cells are entrapped in interpillar space, adhered to micropillar sidewalls, and elongated. Because of the micropillar confinement, cells are confined to elongate either in horizontal or vertical directions. In isotropic micropillar arrays cells elongated in both directions, whereas anisotropic pillar arrays guided cells to elongate in the stiffer direction. c) Scanning electron microscope (SEM) image (pseudo-colored, cells: red, pillars: brown, substrate bottom surface: gray) of a single elongated human mesenchymal stem cell (hMSC) entrapped within an anisotropic interpillar space. (i–iii) Close-up images of the elongated cell in the interpillar space revealed pillar deflection caused by cellular attachment.

unidirectional alignment and elongation in the stiffer direction (Figure 1b). Cell nuclei also aligned in the same direction (Figure 1a,b). Furthermore, cells were observed to be entrapped in the interpillar space and they displayed adhesion to the sidewalls of the pillars as expected (Figure 1c and Figure S3a, Supporting Information). Scanning electron microscopy (SEM) imaging revealed and confirmed bending of micropillars in the compliant direction by the cells due to cell attachment forces (Figure 1c and Figure S3b, Supporting Information).

Micropillar arrays were fabricated using standard clean room microfabrication techniques, which include photolithography, soft lithography, and microcontact printing (**Figure 2**).[29,32–34] Briefly, a positive template composed of pillar structures was obtained by transferring micropatterns from a photomask to a photoresist material coated on a silicon wafer via ultra-violet light (Figure 2a). A negative template consisting of pits and the final micropillar arrays were realized via poly(dimethylsiloxane) (PDMS) casting (Figure 2a). Pillar top surfaces were rendered nonadhesive for cells or proteins through stamping with a pluronics adsorbed PDMS block (Figure 2b). Sidewalls of the micropillars were functionalized to be adhesive for cells by immersing micropillar arrays in fibronectin (FN) solution (Figure 2b). FN, a critical component of ECM, binds to integrin receptors on cell membrane and is a key modulator of cell adhesion.[35,36] Using photolithography and soft lithography, micropillar structures with isotropic and anisotropic geometries, ranging from 7.6×7.7 to 3.9×7.8 µm (Figure 2c,i,ii) and 5.7×5.7 to 5.7×3.7 µm (Figure 2c,iii,iv), were fabricated.

Mechanical properties of fabricated micropillar structures were characterized by reconstructing 3D pillar models from SEM images (**Figure 3**). Area moment of inertia in x- and y-directions for each micropillar geometry was measured using 3D micropillar models. Direction dependent stiffness of each micropillar geometry was calculated using the beam deflection equation.[37] SA was defined as a ratio of stiffness in x-direction to stiffness in y-direction (Figure 3). Micropillar structures with square geometries displayed an SA of 1, whereas rectangular geometries resulted in SA values of up to 3.7 (Figure 3). Moreover, we designed and fabricated micropillar arrays with similar SA, but with lower stiffness values by reducing the dimensions of pillars

ADVANCED HEALTHCARE MATERIALS
www.advhealthmat.de
www.MaterialsViews.com

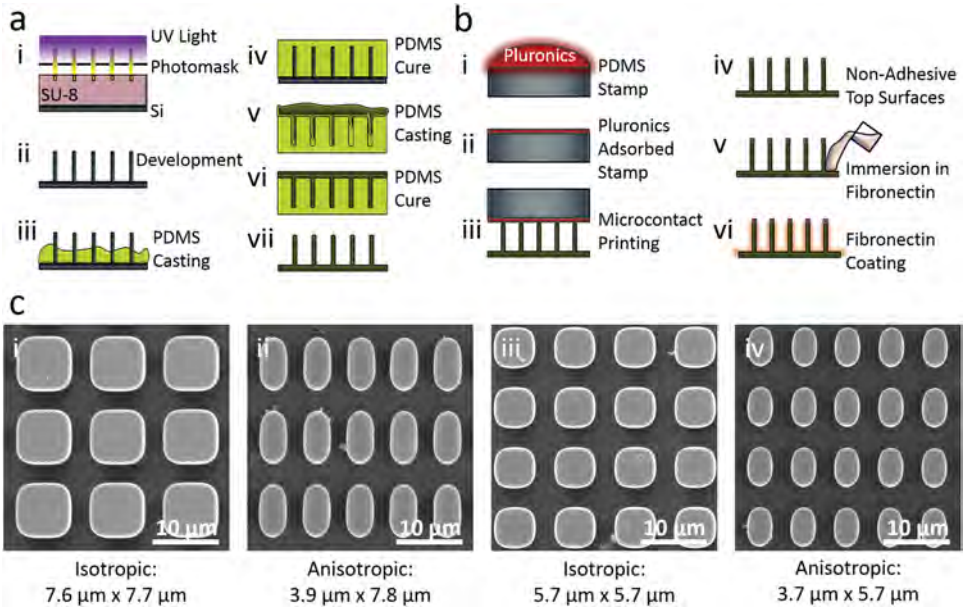

Figure 2. Fabrication, surface modification, and SEM imaging of micropillars. a) Micropillar fabrication: (i) Positive template fabrication using a photoresist material (SU-8) on a silicon (Si) wafer through photolithography, (ii) development of photoresist, (iii) first PDMS casting for negative template, (iv) first PDMS curing, (v) second PDMS casting, (vi) second PDMS curing, and (vii) micropillar arrays. b) Surface modification: (i) Incubation of a nonadhesive coating (Pluronics F127) on a PDMS stamp, (ii) pluronics adsorption on stamp, (iii,iv) microcontact printing for pluronics transfer to micropillar top surfaces, and (v) immersion of micropillar arrays in fibronectin for (vi) functionalization of micropillar sidewalls. c) Fabricated (i,iii) isotropic and (ii,iv) anisotropic micropillar arrays were imaged using SEM after fabrication and their dimensions were quantified.

while keeping the aspect ratios the same. These results showed that bending stiffness and SA of micropillar arrays can be tuned differentially via modification of pillar geometry and dimensions.

Next, we analyzed alignment of hMSCs and cardiomyocytes in isotropically and anisotropically stiff micropillar arrays (**Figure 4**). We observed cell entrapment in interpillar

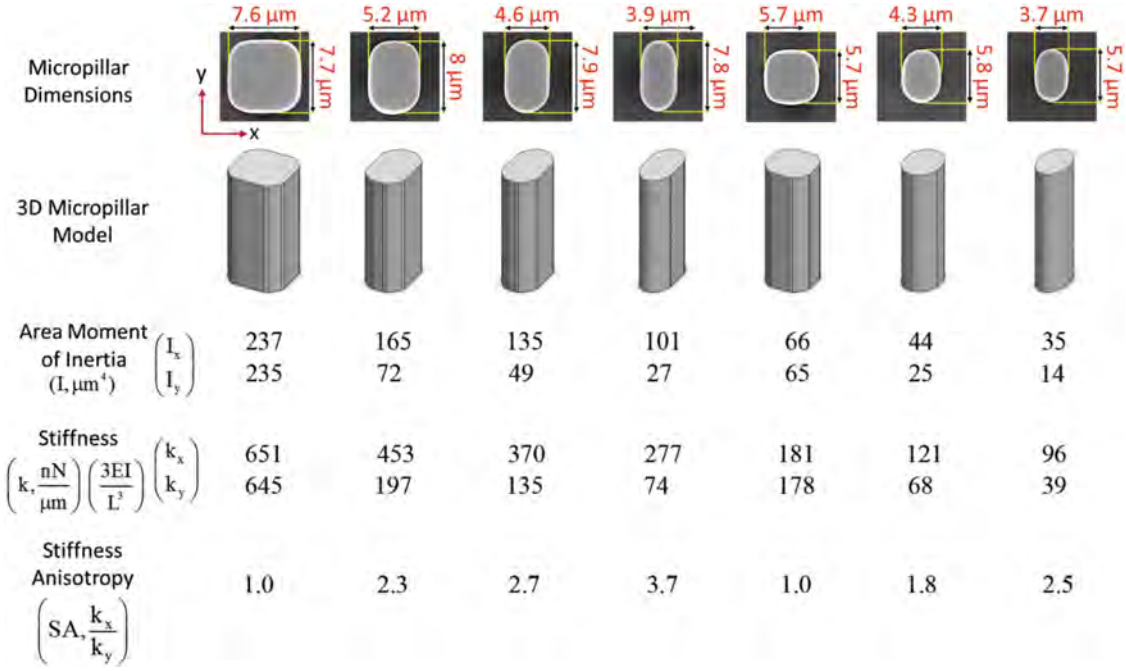

Area Moment of Inertia $(I, \mu m^4)$	I_x	237	165	135	101	66	44	35
	I_y	235	72	49	27	65	25	14
Stiffness $\left(k, \frac{nN}{\mu m}\right)\left(\frac{3EI}{L^3}\right)$	k_x	651	453	370	277	181	121	96
	k_y	645	197	135	74	178	68	39
Stiffness Anisotropy $\left(SA, \frac{k_x}{k_y}\right)$		1.0	2.3	2.7	3.7	1.0	1.8	2.5

Figure 3. Mechanical properties of micropillars determined via 3D reconstruction of micropillar models from SEM images in a computer-aided design (CAD) software**.** The model was utilized for calculation of the area moment of inertia (*I*) in *x*- and *y*-directions for each micropillar design. Pillar stiffness (*k*) in both *x*- and *y*-directions for each design were calculated using stiffness formula for pure bending. SA was calculated by taking the ratio of pillar stiffness in *x*-direction (k_x) to *y*-direction (k_y).

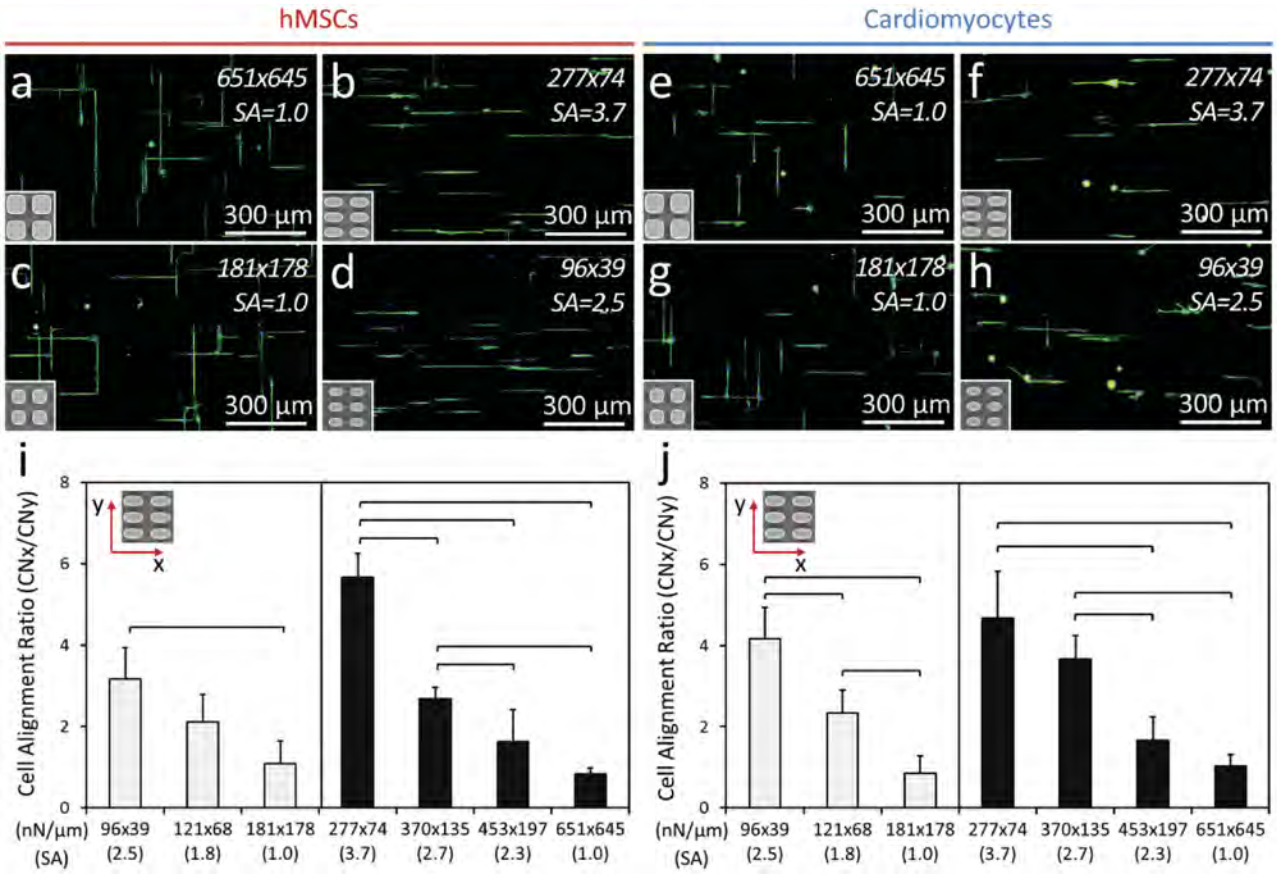

Figure 4. Functionalized anisotropic micropillar arrays control cell morphology and alignment. First, cells are guided to interpillar spaces by the applied nonadhesive surface chemistry to pillar top surfaces and functionalization of pillar sidewalls with fibronectin. Afterwards, anisotropically stiff micropillars guide cells to align in the stiffer direction. a–h) Cell alignment in a,c,e,g) isotropic and b,d,f,h) anisotropic micropillar arrays was observed for a–d) hMSCs and e–h) cardiomyocytes, indicated by cytoskeletal F-actin and nuclear staining. Cells cultured in micropillar arrays displayed a needle-like morphology. Isotropic micropillar arrays showed random cell alignment in both horizontal and vertical directions, whereas cells in anisotropic micropillar arrays unidirectionally aligned in the stiffer (horizontal) direction. i,j) Higher cell alignment ratios (CN_x/CN_y; number of cells aligned in x-direction, CN_x, divided by number of cells in y-direction, CN_y) were observed with increasing stiffness anisotropy of the micropillar arrays for both i) hMSCs and j) cardiomyocytes. General linear model statistical analysis showed a significant association between cell alignment ratio and stiffness anisotropy both for hMSCs and cardiomyocytes ($p < 0.001$ and $p < 0.001$, respectively), whereas there was not any significant association between cell alignment ratio and stiffness for hMSCs and cardiomyocytes ($p = 0.160$ and $p = 0.108$, respectively). The horizontal lines between individual groups represent statistically significant difference based on one-way ANOVA test with Fisher's post hoc test for multiple comparisons ($p < 0.05$). Error bars represent the standard deviations of the means.

spaces both for hMSCs (Figure 4a–d) and cardiomyocytes (Figure 4e–h) in both isotropically (Figure 4a,c,e,g) and anisotropically (Figure 4b,d,f,h) stiff micropillar arrays. Cells in micropillar arrays assumed a needle-like morphology after elongation. Both hMSCs (Figure 4b,d) and cardiomyocytes (Figure 4f,h) displayed predominantly unidirectional alignment and elongation in the stiffer (horizontal) direction of the anisotropically stiff micropillar substrates. However, cell alignment varied randomly in horizontal and vertical directions for isotropically stiff micropillar substrates (Figure 4a,c,e,g).

We calculated unidirectional cell alignment as the number of cells aligned in the stiffer (x-) direction divided by the number of cells in the softer (y-) direction. We observed higher degree of unidirectional cell alignment with increasing SA of the micropillar arrays both for hMSCs (Figure 4i) and cardiomyocytes (Figure 4j). Micropillar arrays with SA of 2.5 and 3.7 (anisotropic) showed significantly greater cell alignment ratios compared to micropillar arrays with SA of 1.0 (isotropic) ($p < 0.05$, one-way analysis of variance (ANOVA) with Fisher's post hoc test). We found a statistically significant association between cell alignment ratio and SA both for hMSCs and cardiomyocytes ($p < 0.05$, ANOVA general linear model, Figure 4i,j). However, there was not any significant association between cell alignment ratio and stiffness neither for hMSCs nor for cardiomyocytes ($p > 0.05$, ANOVA general linear model test). These results show the control of cell alignment and elongation using 3D micropillar arrays via modulation of stiffness anisotropy.

Shape anisotropy is defined as the ratio of the length to the width for cells and their nucleus. The width of cells and their nucleus were equal to interpillar spacing, due to lateral confinement, and length of cells were measured from fluorescent microscope images (Figure S4, Supporting Information). We

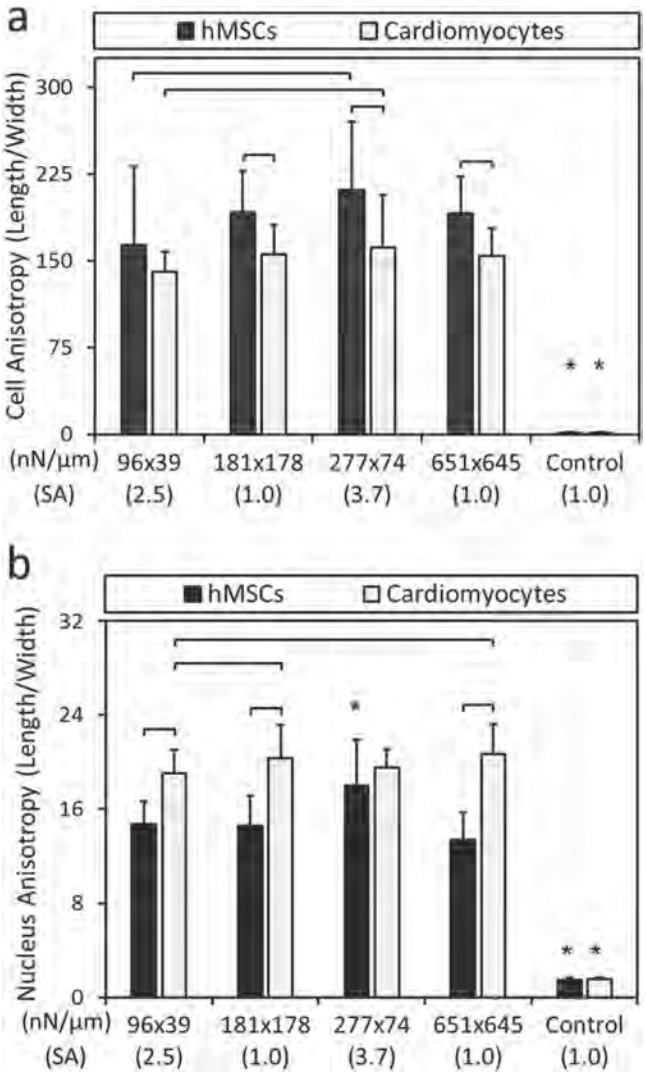

Figure 5. Micropillar arrays induce cell and nucleus shape anisotropy for hMSCs and cardiomyocytes. a) In every group cell shape anisotropy of hMSCs was significantly higher than cardiomyocytes in micropillar arrays. On average, cells in micropillar arrays displayed over 100 times more cell shape anisotropy compared to cells in the control group (flat 2D PDMS, SA of 1.0). b) Cardiomyocytes displayed significantly higher nucleus shape anisotropy in micropillar arrays, whereas there was no significant difference between hMSCs and cardiomyocytes in the control group. Nucleus shape anisotropy of hMSCs reached to a maximum (indicated with*) in the micropillar array with highest stiffness anisotropy (3.7). Nucleus shape anisotropy of the cells cultured in micropillar arrays was up to 15 times more than cells cultured in the control group. The horizontal lines between individual groups represent statistically significant difference based on one-way ANOVA test with Fisher's post hoc test for multiple comparisons ($p < 0.05$). * denotes statistically significant difference between indicated group with other groups for the same cell type. Error bars represent the standard deviations of the means.

analyzed changes in cellular and nuclear shape anisotropy with changing stiffness and SA. Cells cultured on flat 2D PDMS substrates, that were prepared using the same protocol for 3D PDMS micropillar substrates, were also included as a control (SA of 1.0) (**Figure 5**). hMSCs showed significantly higher cell shape anisotropy compared to cardiomyocytes in micropillar arrays ($p < 0.05$, one way ANOVA with Fisher's post hoc test, Figure 5a). On average, cells in micropillar arrays showed over 100-fold greater shape anisotropy compared to cells on 2D PDMS substrates (Figure 5a). Cardiomyocytes displayed significantly higher nucleus shape anisotropy compared to that of hMSCs in micropillar arrays ($p < 0.05$, one way ANOVA with Fisher's post hoc test, Figure 5b). However, there was not any significant difference in nucleus shape anisotropy between hMSCs and cardiomyocytes on 2D PDMS substrates ($p > 0.05$, one way ANOVA with Fisher's post hoc test, Figure 5b). Overall, cells in micropillar arrays displayed up to 15 times greater nucleus shape anisotropy compared to cells on 2D PDMS substrates (Figure 5b). These results show that anisotropically stiff micropillar arrays provide a new and innovative platform to induce cell and nucleus shape anisotropy for hMSCs and cardiomyocytes.

Next, we analyzed entrapment, elongation, and alignment process of cells seeded on anisotropically stiff micropillar arrays (SA of 2.3) over time, from 0.6 to 15 h (**Figure 6** and Figure S5 and Video S1, Supporting Information). Seeded hMSCs settled down on micropillar arrays and started migrating into the interpillar space (Figure 6a). Cells displayed elongation both in stiffer and softer direction within 3–5 h and were fully elongated and aligned in the stiffer direction within 15 h after cell seeding (Figure 6b–d). Quantification of cell length in stiffer and softer directions over time showed a continuous cell elongation in stiffer direction (Figure 6e). However, cell length in softer direction increased within 0.6–5 h but decreased from 5 to 15 h after cell seeding (Figure 6e). These results show the feasibility of anisotropically stiff micropillar arrays for dynamic study of cell behavior, such as stiffness sensing and guiding, in a 3D microenvironment.

Alignment of cellular microenvironment is critical in healthy functioning of numerous tissues and disease progression. Multiple cell types in human body require a functional aligned microenvironment, including endothelial cells lining the inner wall of blood vessels and cardiomyocytes producing necessary force through synchronized contraction.[38] In native cardiac tissues, cardiomyocytes are highly aligned and elongated, with an average length of about 100–160 μm.[39–41] This elongated and aligned organization enables them to provide the synchronized contraction and beating function of the heart. On the other hand, intravasation and extravasation of metastatic cancer cells or leukocytes through blood vessels take place in a highly aligned microenvironment formed by endothelial cells, smooth muscle cells, pericytes, and, to some extent, macrophages.[38,42] Furthermore, increased alignment of surrounding collagen perpendicular to tumors, especially in breast carcinoma, has been shown to be a critical feature for cell migration out of the tumor.[43,44] Even though presented micropillar system would not be able to capture every aspect of these in vivo phenomena, it holds great potential as an in vitro model by allowing precise control of the microenvironment for mechanistic studies of cell response to change in a particular property.

The presented micropillar system provides a modality to not only elongate cells up to 500 μm (Figure S4, Supporting Information) but also align them unidirectionally. In our study, the extraordinary cell elongation in the micropillar arrays occurs due to cell migration to the interpillar space and confinement of

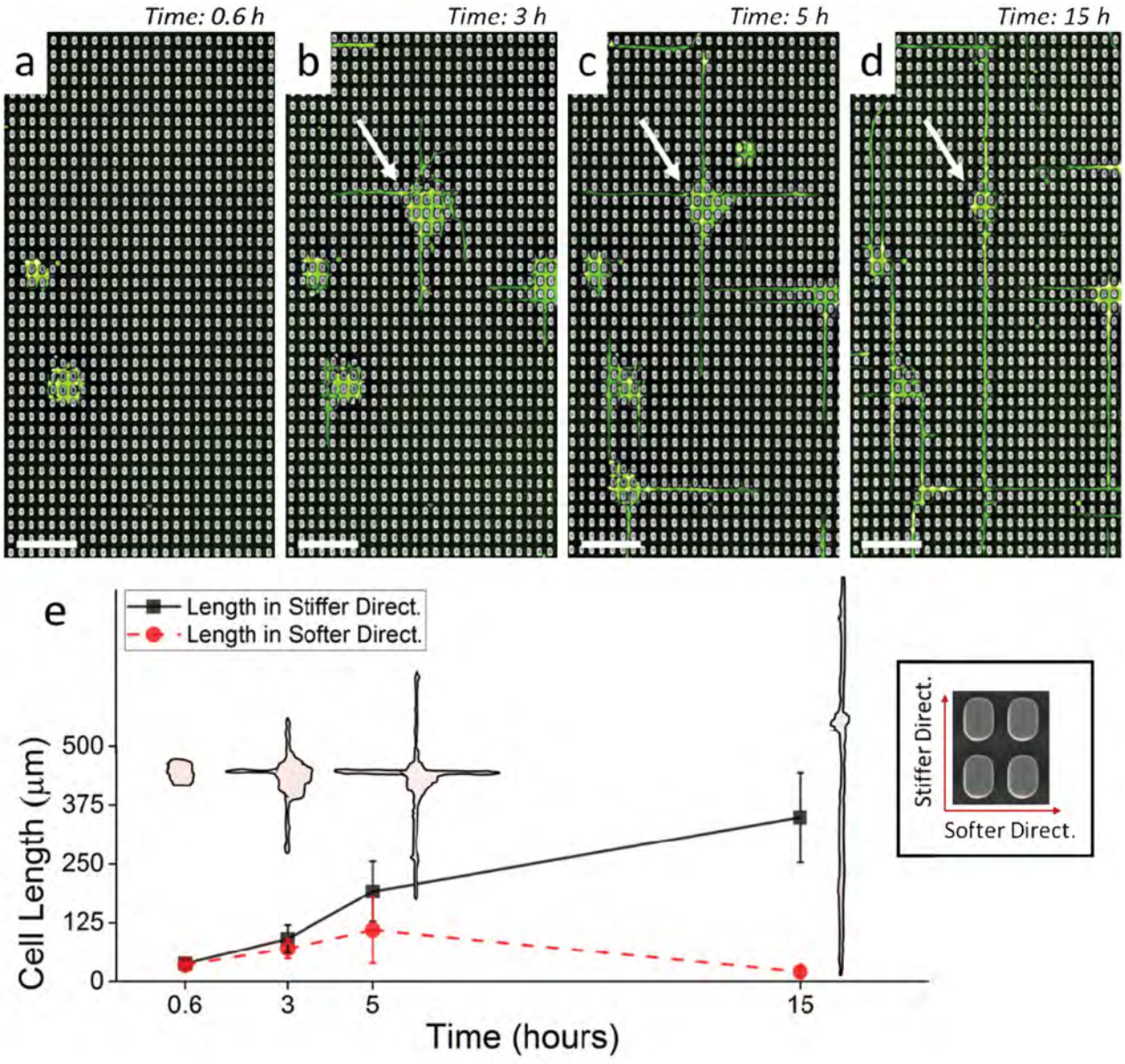

Figure 6. Time lapse analysis of cell entrapment and elongation in interpillar space. a) Seeded hMSCs settled down on anisotropically stiff micropillar arrays (SA = 2.3) and started migrating into the interpillar space. b,c) Cell elongation in interpillar space began within 3–5 h after cell seeding. d) Cells were fully elongated and aligned in the stiffer direction (vertical) within 15 h after cell seeding. White arrow points to a typically elongated cell. Scale bars indicate 50 µm of length. e) Cell length in softer direction increased within 0.6–5 h but decreased from 5 to 15 h after seeding. On the other hand, cell length in stiffer direction displayed a continuous increase within 15 h after seeding. Schematic of a typical cell morphology over time is displayed in the plot. Inset shows stiffer and softer directions in the micropillar array. Error bars represent standard deviations of the means ($n = 7$ cells at each time point).

cell attachment process within the pillar side walls. This purely guided entrapment process took place equally well both for isotropic and anisotropic pillar arrays. On the other hand, our results showed that alignment of cells in 3D microenvironment is a function of stiffness anisotropy. Others have investigated the effects of substrate topography and stiffness on elongation of different cell types. Microgrooves have been utilized in the literature for unidirectional alignment and elongation of cells, where groove structures with a low depth (<3 µm) acting as a 2D substrate, providing contact guidance to cells.[19,45–49] Other than microgrooves, Ghibaudo and co-workers used anisotropically stiff micropillars as a 2D semicontinuous substrate to align and elongate fibroblasts.[31] In most of these studies performed on 2D microfabricated substrates, cell elongation in the range of 50–200 µm was reported.[19,31,45,49] In comparison, our results demonstrated that cells were confined in the 3D micropillar environment and displayed more than twofold greater elongation.

A point of discussion associated with the presented micropillar approach, as well as most anisotropically stiff microstructures, is that mechanical stiffness is inherently coupled to structural geometry, which causes a discrepancy in the surface

areas for stiff and compliant directions such that the stiffer direction presents more surface area for cell adhesion which in turn may arguably act as a cue for cells to elongate along the stiffer direction. Therefore, differences in surface areas might confound the effect of stiffness anisotropy. The time lapse analysis of cell elongation (Figure 6e) appears to rule out surface area to be a cause of cellular elongation because cells elongate along both directions within 5 h. Only by 15 h the stiffer axis dominates as the cell elongation and alignment direction. If such a confounding effect of surface area on cell elongation was indeed in play, it would have prevented elongation in compliant direction in the initial stages.

Differential functionalization of micropillar top surfaces as nonadhesive and sidewalls as adhesive allowed cell migration to the interpillar space and entrapment of the cell attachment processes. However, a shortcoming of this functionalization approach is the lack of specificity that would allow functionalization of only pillar sidewalls or a certain portion of the sidewalls. Despite this limitation, based on the SEM images (Figure 1c and Figure S3, Supporting Information), cell adhesion to base surface was limited. Cells either covered pillar sidewall extensively or adhered to the middle portion of the pillars. Bending stiffness of the pillar structures depends on area moment of inertia, Young's Modulus, and length of the pillars. We used total length of the pillars for calculating the nominal micropillar stiffness. Even though cells mostly adhere from the mid region of the micropillar sidewalls, relative ratio of bending stiffness among isotropic and anisotropic pillar arrays would not be affected, since applied length is same for all pillar arrays.

Actomyosin contractility is one of the main driving forces behind cell shape changes and elongation.[50,51] It has been suggested that higher levels of actomyosin contraction of cells can be observed in confined 3D environments in comparison to 2D surfaces, since cell detachment is not possible.[52] In this study, we developed a microfabricated platform with controlled mechanical, chemical, and biological properties to study cell morphology, alignment, and elongation in a confined 3D microenvironment. Indeed, previously, an elongation around 60 μm was shown for fibroblasts cultured on top surfaces (2D) of micropillars with a SA of 4.0,[31] which is fivefold to eightfold lower than the results reported here.

Migration is an essential component of physiological functioning for cells and tissues, as well as for pathology of many diseases, such as metastatic cancer. However, cell migration behavior in 3D environments fundamentally differs than on 2D substrates,[52–54] which were commonly used for migration studies in the literature. In time lapse analyses, we observed migration of single MSCs, albeit limited, from 2D flat surface to 3D micropillar environment, or within the 3D micropillar environment (Figure S6, Supporting Information). These results establish the proof-of-concept for migration in 3D micropillar arrays and indicate the potential of 3D micropillar substrates as a platform for cell migration studies or as a disease-on-a-chip model, such as for cancer metastasis.

Tissue engineering aims to cultivate and enrich cells in vitro and to transform them into functional tissue constructs via engineered substrates and bioinductive molecules.[55] In vivo, different tissues present specific mechanical, electrical, and biochemical functional organizations.[38,55–58] Cells in neural, vascular, and muscle tissues display uniaxially aligned and elongated organization, which is critical for their function.[38,55,59] For example, highly aligned and elongated cardiomyocytes are needed in cardiac tissue engineering to achieve a functional tissue organization.[8,55] Directing MSC fate using substrate topography and stiffness has been shown pervasively in the literature.[5,8,13,58,60] Kishore et al. showed tenogenic differentiation of MSCs cultured on electrochemically aligned collagen threads, on which cells displayed an elongated and aligned morphology.[13] Similarly, myogenic and neurogenic differentiation of elongated and aligned MSCs on substrates with micro/nano grooves was reported.[8,61] Furthermore, effect of cell morphology, such as elongation, on modulation of epigenetic state and mesenchymal-to-epithelial transition of adult fibroblasts was shown on microgroove substrates.[47]

Nucleus is the largest and stiffest cell organelle and it is exposed to mechanical forces transmitted through the cytoskeleton from the outside and also the forces generated within the cell. It has been shown that nuclear structural elements, as well as cytoskeleton, are dynamically reconstructed in response to force.[62–64] Moreover, change in cell phenotype during differentiation has been associated with nuclear morphology and stiffness, as well as tumor cell differentiation and metastasis potential.[64] In embryonic stem cells, histone acetylation and methylation have been shown to alter chromatin plasticity and differentiation characteristics.[65] Cell entrapment in 3D micropillar arrays can be utilized for controlled deformation of cell nucleus to study nuclear mechanics and mechanotransduction pathways in stem cell differentiation.

The results presented in this paper establish the groundwork of a new approach and platform that would allow the study of cell behavior in a precisely controlled 3D microenvironment. The described microfabricated pillar system can be utilized for the study of cell–ECM interactions and cell behavior in a mechanically controlled 3D environment for different cell types, including hMSCs and cardiomyocytes. The micropillar platform allows precise control over substrate stiffness and stiffness anisotropy, which induces different degree of cell alignment and elongation. We will utilize these unique capabilities of the micropillar platform to study the effect of extraordinary elongation and alignment on cell behavior, such as differentiation and reprogramming, in future studies. The presented microengineered approach induces cells to elongate and align along the stiffer axes of micropillars while confining cells in a 3D environment. Cultivation of highly elongated and aligned cardiomyocyte constructs can potentially lead to a highly organized and functional cardiac tissue. Furthermore, highly organized cell arrays can be utilized in other tissues with elongated cell phenotypes, such as nerves, tendons, and ligaments.

Experimental Section

Micropillar Fabrication: Micropillar arrays were fabricated based on photolithography and soft lithography. A positive template on a silicon wafer, consisting an array of pillars, was fabricated using photolithography and wet chemical development. Positive template was silanized with (tridecaf luoro-1,1,2,2-tetrahydrooctyl)-1-trichlorosilane (United Chemical Technologies, Bristol, PA) vapor under vacuum to facilitate separation of molded polymer from the template. Next, the PDMS (Sylgard 184,

Ellsworth Adhesives, Germantown, WI) prepolymer (10:1 weight ratio) was poured over the positive template, cured at 110 °C for 15 min, and peeled off, resulting in a negative PDMS template. The negative template was treated under UV ozone cleaner (Novascan PSDP-UV8T) for 10 min at 90 °C and silanized under vacuum. Afterwards, PDMS prepolymer (10:1 weight ratio) was molded into the negative template, degassed under vacuum, pressed against a coverslip, cured at 110 °C for 22 h, and peeled off from the negative template, producing micropillar arrays. This process yielded the micropillar arrays on a coverslip.

Mechanical Characterization of Micropillars: 3D models of fabricated micropillars were reconstructed from SEM images and area moment of inertia of every pillar structure was measured using SolidWorks (Dassault Systèmes, Vélizy-Villacoublay, France). Bending stiffness of micropillars was calculated using beam deflection Equation (1)

$$k = \left(\frac{3EI}{L^3}\right) \quad (1)$$

where k is the stiffness, E is the Young's Modulus, I is the area moment of inertia, and L is the pillar length. Young's modulus was determined from the slope of tensile stress–strain curve of PDMS strips obtained from the substrate used in the fabrication of micropillars. Stiffness anisotropy (k_x/k_y) of micropillars was calculated as the ratio of stiffness in x-direction (k_x) to stiffness in y-direction (k_y).

Surface Chemistry: Top surfaces of micropillars were treated to be nonadhesive for cells using microcontact printing. Prepolymer of PDMS (30:1 weight ratio) was molded in a cell culture dish and cured for 2 h at 60 °C. Next, cured PDMS was cut into blocks and peeled off from the cell culture dish, resulting in PDMS stamps. Afterwards, Pluronic F127 (1%, Sigma-Aldrich, St. Louis, MO) in distilled water was adsorbed on the flat surface of the stamps. Stamps were placed in a conformal contact with the micropillar arrays for transferring Pluronic F127 to prevent cell adhesion on micropillar top surfaces. Furthermore, remaining unstamped surfaces of micropillar arrays, such as micropillar sidewalls, were functionalized with FN (Sigma-Aldrich, St. Louis, MO) by immersing the whole array in a FN solution (37.5 μg mL^{-1}) for 1 h.

Cell Culture on Micropillar Arrays: Sterilized samples were placed in cell culture dishes (≈30 cm^2 area). Culture medium was α-Minimum Essential Medium (MEM) supplemented with fetal bovine serum (10%, FBS) (Life technologies, Grand Island, NY) containing penicillin (100 U mL^{-1}), and streptomycin (100 μg mL^{-1}). Media (5 mL) was added on top of each sample. Passage three bone marrow-derived hMSCs was suspended in medium and applied dropwise, using a pipettor from a distance of about 2 cm height, on top of each sample uniformly with a density of 2000 cell cm^{-2}. Immortalized cardiomyocytes at passage 18 were seeded on another set of samples with the same approach. Cell seeded samples were incubated in an atmosphere control incubator at 37 °C under 5% carbon dioxide atmosphere for 20 h.

Microscopy and Data Analysis: After 20 h of culture, samples were rinsed in 1X phosphate buffered saline (PBS) and fixed with glutaraldehyde in PBS (2%) for 20 min. For SEM imaging, samples were dehydrated in ethanol in with serial dilution and then critical point dried (CPD 030, Bal-Tec AG, Balzers, Liechtenstein) under CO_2. Samples were coated with palladium in a sputter coating device and imaged with an SEM (FEI Helios 650, Hillsboro, OR). For fluorescent microscopy, samples were rinsed with 1X PBS and were fixed with phosphate buffered formalin (10%, Fisher Scientific, Waltham, MA) and stained with Alexa Fluor 488 and DAPI (Life technologies, Grand Island, NY) for actin filament and nucleus fluorescent staining, respectively. Fluorescent and phase contrast imaging was performed with an Olympus IX83 inverted motorized microscope with Olympus Cell Sense imaging and analysis software (Olympus Corp., Tokyo, Japan). An Olympus 10X (numerical aperture: 0.3) objective was utilized for image recording. Cell alignment, cell length and width, cell shape anisotropy, and cell nucleus shape anisotropy were quantified using ImageJ software (National Institute of Health, US). Cell and nucleus elongation were measured as the longest axis of the cell body and nucleus within the interpillar space. Cell shape anisotropy was quantified by measuring the longest axis of the cell body divided to the shorter axis.

Time Lapse Analysis of Cell Entrapment, Elongation, and Alignment: Fluorescent cell tracking staining kit was purchased from Abcam (CytoPainter Cell Tracking Stain Kit, ab138891, Cambridge, MA). 200 000 cells were suspended in of media (400 μL). Staining solution (400 μL) was prepared via diluting the stain with assay buffer with a ratio of 1:500. Stain was added to cell suspension and cells were incubated in an incubator at 37 °C and 5% CO_2 for 20 min. Cell solution was centrifuged and pelleted at 1200 rpm for 5 min and then suspended in media (1 mL). Micropillars arrays were placed in a cell culture dish (28 cm^2 area) with growth media (5 mL, α-MEM supplemented with 10% FBS containing penicillin (100 U mL^{-1}) and streptomycin (100 μg mL^{-1})). Cells suspension was added to culture media dropwise, using a pipettor from a distance of about 2 cm height, on top of the micropillars with a cell density of 2000 cell cm^{-2}. Cells were imaged with fluorescent microscope at different time points of 0.6, 3, 5, and 15 h after cell seeding to visualize cell entrapment, elongation, and alignment in 3D interpillar space.

Statistical Analysis: Data obtained in this study were reported as mean ± standard deviation. General linear model statistical analysis was performed to analyze association of cell alignment ratio with stiffness anisotropy and stiffness. Based on the general linear model analysis results, effect of stiffness anisotropy on cell alignment ratio was statistically analyzed using one-way ANOVA test. Cell shape anisotropy and cell nucleus shape anisotropy were statistically assessed (Minitab 16 software, Minitab Inc., State College, PA) using ANOVA with Fisher's post hoc test for multiple comparisons. Statistical significance is set at 95% confidence level for all tests ($p < 0.05$). Error bars in figures represent the standard deviations of the means.

Supporting Information

Supporting Information is available from the Wiley Online Library or from the author.

Acknowledgements

Y.A. and M.Y. contributed equally to this work. This work was supported by Grant No. 2013126 from the Doris Duke Charitable Foundation, Grant No. R01 AR063701 from the National Institute of Health, and Grant No. DMR-1306665 from the National Science Foundation. Authors acknowledge Grace Gongaware from Case Biomanufacturing and Microfabrication Laboratory and Cleveland Institute of Art for pseudo-coloring the SEM images and for crafting the scientific illustration. U. A. G. would like to thank the Case Western Reserve University, University Center for Innovation in Teaching and Education (UCITE) for the Glennan Fellowship, which supports the scientific art program and the art student internship in Case Biomanufacturing and Microfabrication Laboratory.

Received: January 27, 2016
Revised: March 10, 2016
Published online: May 18, 2016

[1] Y. Sun, S. Chen, *Annu. Rev. Biophys.* **2012**, *41*, 519.
[2] Y. Sun, Q. Jallerat, M. Szymanski, A. W. Feinberg, *Nat. Methods* **2015**, *12*, 134.
[3] L. Wang, Y. Li, B. Chen, S. Liu, M. Li, L. Zheng, P. Wang, T. J. Lu, F. Xu, *ACS Appl. Mater. Interfaces* **2015**, *7*, 15088.
[4] J. Y. Lim, H. J. Donahue, *Tissue Eng.* **2007**, *13*, 1879.
[5] R. Peng, X. Yao, J. Ding, *Biomaterials* **2011**, *32*, 8048.
[6] A. Saez, M. Ghibaudo, A. Buguin, P. Silberzan, B. Ladoux, *Proc. Natl. Acad. Sci. USA* **2007**, *104*, 8281.

[7] J. Fu, Y. K. Wang, M. T. Yang, R. A. Desai, X. Yu, Z. Liu, C. S. Chen, *Nat. Methods* **2010**, *7*, 733.
[8] C. Y. Tay, H. Yu, M. Pal, W. S. Leong, N. S. Tan, K. W. Ng, D. T. Leong, L. P. Tan, *Exp. Cell Res.* **2010**, *316*, 1159.
[9] P. Y. Wang, J. Yu, J. H. Lin, W. B. Tsai, *Acta Biomater.* **2011**, *7*, 3285.
[10] J. S. Choi, S. J. Lee, G. J. Christ, A. Atala, J. J. Yoo, *Biomaterials* **2008**, *29*, 2899.
[11] L. F. Tseng, P. T. Mather, J. H. Henderson, *Acta Biomater.* **2013**, *9*, 8790.
[12] S. Y. Chew, R. Mi, A. Hoke, K. W. Leong, *Biomaterials* **2008**, *29*, 653.
[13] V. Kishore, W. Bullock, X. Sun, W. S. Van Dyke, O. Akkus, *Biomaterials* **2012**, *33*, 2137.
[14] M. Younesi, A. Islam, V. Kishore, J. M. Anderson, O. Akkus, *Adv. Funct. Mater.* **2014**, *24*, 5762.
[15] M. A. Bucaro, Y. Vasquez, B. D. Hatton, J. Aizenberg, *ACS Nano* **2012**, *6*, 6222.
[16] B. W. Tuft, S. Li, L. Xu, J. C. Clarke, S. P. White, B. A. Guymon, K. X. Perez, M. R. Hansen, C. A. Guymon, *Biomaterials* **2013**, *34*, 42.
[17] D. H. Kim, E. A. Lipke, P. Kim, R. Cheong, S. Thompson, M. Delannoy, K. Y. Suh, L. Tung, A. Levchenko, *Proc. Natl. Acad. Sci. USA* **2010**, *107*, 565.
[18] L. E. Dickinson, D. R. Rand, J. Tsao, W. Eberle, S. Gerecht, *J. Biomed. Mater. Res. A* **2012**, *100*, 1457.
[19] A. I. Teixeira, G. A. Abrams, P. J. Bertics, C. J. Murphy, P. F. Nealey, *J. Cell. Sci.* **2003**, *116*, 1881.
[20] B. Koch, S. Sanchez, C. K. Schmidt, A. Swiersy, S. P. Jackson, O. G. Schmidt, *Adv. Healthcare Mater.* **2014**, *3*, 1753.
[21] W. R. Legant, J. S. Miller, B. L. Blakely, D. M. Cohen, G. M. Genin, C. S. Chen, *Nat. Methods* **2010**, *7*, 969.
[22] M. Unal, Y. Alapan, H. Jia, A. G. Varga, K. Angelino, M. Aslan, I. Sayin, C. Han, Y. Jiang, Z. Zhang, U. A. Gurkan, *Nanobiomedicine* **2014**, *1*, 59379.
[23] M. Ghibaudo, J. M. Di Meglio, P. Hersen, B. Ladoux, *Lab Chip* **2011**, *11*, 805.
[24] M. Marelli, N. Gadhari, G. Boero, M. Chiquet, J. Brugger, *Lab Chip* **2014**, *14*, 286.
[25] M. Ochsner, M. Textor, V. Vogel, M. L. Smith, *PLoS One* **2010**, *5*, e9445.
[26] E. Cukierman, R. Pankov, D. R. Stevens, K. M. Yamada, *Science* **2001**, *294*, 1708.
[27] B. Koch, A. K. Meyer, L. Helbig, S. M. Harazim, A. Storch, S. Sanchez, O. G. Schmidt, *Nano Lett.* **2015**, *15*, 5530.
[28] W. Xi, C. K. Schmidt, S. Sanchez, D. H. Garcias, R. E. Carazo-Salas, S. P. Jackson, O. G. Schmidt, *Nano Lett.* **2014**, *15*, 5530.
[29] J. L. Tan, J. Tien, D. M. Pirone, D. S. Gray, K. Bhadriraju, C. S. Chen, *Proc. Natl. Acad. Sci. USA* **2003**, *100*, 1484.
[30] A. Rabodze, P. Alcaide, F. W. Luscinskas, B. Ladoux, *Biophys. J.* **2008**, *95*, 1428.
[31] M. Ghibaudo, A. Saez, L. Trichet, A. Xayaphoummine, J. Browaeys, P. Silberzan, A. Buguin, B. Ladoux, *Soft Matter* **2008**, *4*, 1836.
[32] M. T. Yang, J. Fu, Y. K. Wang, R. A. Desai, C. S. Chen, *Nat. Protoc.* **2011**, *6*, 187.
[33] M. T. Yang, N. J. Sniadecki, C. S. Chen, *Adv. Mater.* **2007**, *19*, 3119.
[34] Y. Alapan, K. Icoz, U. A. Gurkan, *Biotechnol. Adv.* **2015**, *33*, 1277.
[35] R. Pankov, K. M. Yamada, *J. Cell Sci.* **2002**, *115*, 3861.
[36] E. Ruoslahti, *Cancer Metastasis Rev.* **1984**, *3*, 43.
[37] F. Beer, E. R. Johnston, J. DeWolf, D. F. Mazurek, *Mechanics of Materials*, McGraw-Hill, NY **2012**.
[38] Y. Li, G. Huang, X. Zhang, L. Wang, Y. Du, T. J. Lu, F. Xu, *Biotechnol. Adv.* **2014**, *32*, 347.
[39] S. Hinrichs, J. Heger, R. Schreckenberg, S. Wenzel, G. Euler, C. Arens, M. Bader, S. Rosenkranz, E. Caglayan, K. D. Schluter, *Cardiovasc. Res.* **2011**, *89*, 344.
[40] M. M. Laks, M. J. Nisenson, H. J. Swan, *Circ. Res.* **1967**, *21*, 671.
[41] A. Fraticelli, R. Josephson, R. Danziger, E. Lakatta, H. Spurgeon, *Am. J. Physiol.* **1989**, *257*, H259.
[42] W. Weninger, M. Biro, R. Jain, *Nat. Rev. Immunol.* **2014**, *14*, 232.
[43] P. Keely, A. Nain, *F1000 Research* **2015**, *4*, 1408.
[44] K. M. Riching, B. L. Cox, M. R. Salick, C. Pehlke, A. S. Riching, S. M. Ponik, B. R. Bass, W. C. Crone, Y. Jiang, A. M. Weaver, K. W. Eliceiri, P. J. Keely, *Biophys. J.* **2014**, *107*, 2546.
[45] C. J. Bettinger, B. Orrick, A. Misra, R. Langer, J. T. Borenstein, *Biomaterials* **2006**, *27*, 2558.
[46] P. Uttayarat, M. Chen, M. Li, F. D. Allen, R. J. Composto, P. I. Lelkes, *Am J Physiol Heart Circ Physiol* **2008**, *294*, H1027.
[47] T. L. Downing, J. Soto, C. Morez, T. Houssin, A. Fritz, F. Yuan, J. Chu, S. Patel, D. V. Schaffer, S. Li, *Nat. Mater.* **2013**, *12*, 1154.
[48] Y. Li, J. S. Chu, K. Kurpinski, X. Li, D. M. Bautista, L. Yang, K. L. Sung, S. Li, *Biophys J* **2011**, *100*, 1902.
[49] I. H. Yang, C. C. Co, C. C. Ho, *Biomaterials* **2005**, *26*, 6599.
[50] M. Murrell, P. W. Oakes, M. Lenz, M. L. Gardel, *Nat. Rev. Mol. Cell Biol.* **2015**, *16*, 486.
[51] I. B. Bischofs, F. Klein, D. Lehnert, M. Bastmeyer, U. S. Schwarz, *Biophys. J.* **2008**, *95*, 3488.
[52] G. Charras, E. Sahai, *Nat. Rev. Mol. Cell Biol.* **2014**, *15*, 813.
[53] G. Reig, E. Pulgar, M. L. Concha, *Development* **2014**, *141*, 1999.
[54] S. I. Fraley, P. H. Wu, L. He, Y. Feng, R. Krisnamurthy, G. D. Longmore, D. Wirtz, *Sci. Rep.* **2015**, *5*, 14580.
[55] T. Dvir, B. P. Timko, D. S. Kohane, R. Langer, *Nat. Nanotechnol.* **2011**, *6*, 13.
[56] E. G. Roberts, E. L. Lee, D. Backman, J. A. Buczek-Thomas, S. Emani, J. Y. Wong, *Ann. Biomed. Eng.* **2015**, *43*, 762.
[57] B. Sharma, J. H. Elisseeff, *Ann. Biomed. Eng.* **2004**, *32*, 148.
[58] N. Thavandiran, S. S. Nunes, Y. Xiao, M. Radisic, *Stem Cell Res. Ther.* **2013**, *4*, 14.
[59] C. J. Bettinger, R. Langer, J. T. Borenstein, *Angew. Chem. Int. Ed. Engl.* **2009**, *48*, 5406.
[60] D. Hoffman-Kim, J. A. Mitchel, R. V. Bellamkonda, *Annu. Rev. Biomed. Eng.* **2010**, *12*, 203.
[61] E. K. Yim, S. W. Pang, K. W. Leong, *Exp. Cell Res.* **2007**, *313*, 1820.
[62] J. Swift, D. E. Discher, *J. Cell Sci.* **2014**, *127*, 3005.
[63] P. Isermann, J. Lammerding, *Curr. Biol.* **2013**, *23*, R1113.
[64] K. N. Dahl, A. J. Ribeiro, J. Lammerding, *Circ. Res.* **2008**, *102*, 1307.
[65] S. Melcer, H. Hezroni, E. Rand, M. Nissim-Rafinia, A. Skoultchi, C. L. Stewart, M. Bustin, E. Meshorer, *Nat. Commun.* **2012**, *3*, 910.